Retrievals of sea surface temperature from infrared imagery: origin and form of systematic errors

Q. J. R. Meteorol. Soc. (2006), **132**, pp. 1205–1223 doi: 10.1256/qj.05.143

Retrievals of sea surface temperature from infrared imagery: origin and form of systematic errors

By C. J. MERCHANT[1]*, L. A. HORROCKS[2], J. R. EYRE[3] and A. G. O'CARROLL[3]

[1]*School of GeoSciences, The University of Edinburgh, UK*
[2]*Department of Environment Food and Rural Affairs, London, UK*
[3]*Met Office, Exeter, UK*

(Received 8 July 2005, revised 17 November 2005)

SUMMARY

We show that retrievals of sea surface temperature from satellite infrared imagery are prone to two forms of systematic error: prior error (familiar from the theory of atmospheric sounding) and error arising from nonlinearity. These errors have different complex geographical variations, related to the differing geographical distributions of the main geophysical variables that determine clear-sky brightness-temperatures over the oceans. We show that such errors arise as an intrinsic consequence of the form of the retrieval (rather than as a consequence of sub-optimally specified retrieval coefficients, as is often assumed) and that the pattern of observed errors can be simulated in detail using radiative-transfer modelling. The prior error has the linear form familiar from atmospheric sounding. A quadratic equation for nonlinearity error is derived, and it is verified that the nonlinearity error exhibits predominantly quadratic behaviour in this case.

KEYWORDS: Advanced Very High Resolution Radiometer (AVHRR) Along-track Scanning Radiometer (ATSR)

1. SCOPE OF PAPER

Sea surface temperature (SST) has been routinely obtained for over two decades from broad-band infra-red radiances observed by sensors on satellites. Generally, following the suggestion of McMillin (1975), radiances are expressed as brightness temperatures (BTs) and the SST estimate is a linear (or nearly linear) combination of these:

$$\widehat{x} = a_0 + \mathbf{a}^{\mathrm{T}}\mathbf{y}^{\mathrm{o}}, \tag{1}$$

where $\widehat{x}$ is the estimated SST, a_0 is an offset coefficient, $\mathbf{a}$ is a column vector of weighting coefficients and $\mathbf{y}^o$ contains the observed BTs.

The coefficients in the retrieval equation may be derived by regression of observed BTs to *in situ* measurements (e.g., McClain *et al.* 1985; Walton *et al.* 1998), or by regression using BTs simulated using radiative-transfer modelling (e.g., Llewellyn-Jones *et al.* 1984; Závody *et al.* 1995). In nearly linear formulations, the coefficients are weak functions of a prior or first-guess SST. This retrieval method is convenient and simple to implement.

Linear retrieval using regression-based coefficients also appears to be conceptually straightforward. The purpose of this paper is to show that this appearance is deceptive. Linear retrieval leads to systematic errors in SST retrievals that have complex spatial and temporal characteristics. In the particular case illustrated in this paper, these errors are generally smaller than 0.3 K. While such errors may in the past have been neglected, our context is determining SST for climate applications: systematic errors of this magnitude are significant, and need to be thoroughly understood. Such systematic errors are also unlikely to remain acceptable for numerical weather prediction in the future.

We proceed as follows. Firstly, we describe empirically the nature of the systematic errors found in a particular satellite SST data set, both in observation and in simulation. A global mean bias is found in the observations, the magnitude of which is readily

* Corresponding author: School of GeoSciences, The University of Edinburgh, UK. e-mail: c.merchant@ed.ac.uk

explained in terms of systematic simulation errors (Merchant and Le Borgne 2004). However, the focus of the present paper is to explain and characterize the complex regional pattern of systematic error that remains after removing this global offset. We show that we are able to reproduce the observed pattern in simulation. In the second part of the paper, we develop the equations describing the systematic errors that arise when linear retrieval is used for estimation of a variable (such as SST) that, along with many other variables (such as the profiles of temperature and water vapour in the atmosphere), is related in a weakly nonlinear way to the observables (such as brightness temperatures). The systematic error will be shown to comprise 'bias to the prior' (hereafter, 'prior error'), which is well known in the meteorological literature on inversion of linear problems (e.g., Eyre 1987), and a term arising from BTs being nonlinearly related to SST and atmospheric state (hereafter, 'nonlinearity error'). The third section then applies those equations to our case study. We demonstrate that the systematic error does have the characteristics predicted by the theory, and show how the geographical variations of SST and atmospheric state are transformed into regional SST biases by the retrieval process. Lastly, we conclude with some further discussion.

2. Observed and simulated systematic error in SST

(*a*) *The SST data*

Global SSTs of a quality suitable for climate applications have been an objective of the Along Track Scanning Radiometers (ATSRs) flown on European research satellites. The first in the series was ATSR, which commenced routine observation in September 1991. At time of writing, the third instrument in this series is operational, the Advanced ATSR (AATSR) on Envisat. We use AATSR observations and simulations as our case study in this paper.

The unique features of the ATSR series, compared to other SST sensors, are their low channel noise (noise equivalent differential temperature, NEΔT, around 0.05 K), their accurate two-point black-body calibration (stable to $\sim$0.03 K over the mission lifetime) and their conical scanning arrangement that gives the sensor two views of every point observed—one nearly vertical (nadir), the other in a forward look direction (around 56° satellite zenith angle). In common with many SST sensors, SST is estimated from the BTs seen by broad thermal infrared channels located in window regions of the atmospheric transmittance spectrum. These channels are nominally centred on wavelengths of 3.7 μm, 11 μm and 12 μm. Of these, the 3.7 μm channel is used for SST estimation only at night, there being the possibility of contamination by reflected solar irradiance during day. Thus, there are different day and night retrieval coefficients, which we refer to respectively as 'dual-view three-channel' (D3) and 'dual-view two-channel' (D2). Of course, both D3 and D2 may be applied to estimate SST at night, and one would wish the SSTs so obtained to be consistent.

Retrieval coefficients for AATSR have been defined following the procedures of Merchant *et al.* (1999). They are based on radiative-transfer modelling of BTs for globally representative 'states' (that is, SSTs and associated atmospheric profiles of temperature and water vapour) extracted from re-analysis fields of the European Centre for Medium-Range Weather Forecasts (ECMWF). The coefficients are obtained by regression of BTs to the state SSTs (subject to a linear constraint designed to make them tolerant to stratospheric aerosol). Here, we use SSTs derived from the standard European Space Agency coefficients*.

* *Envisat Products Handbook*, http://envisat.esa.int/dataproducts/

Early-release AATSR data at 10 arc-minute spatial resolution were provided to the Met Office as part of the Envisat calibration-validation programme. Retrieved SSTs were collocated with *in situ* measurements of SST from buoys for the one-year period 19 August 2002 to 19 August 2003. D2 SSTs were biased (relative to *in situ* SST corrected for cool-skin effect) by 0.053 ± 0.008 K (mean $\pm$ standard error in mean), whereas D3 SSTs, on the same data, are biased by 0.219 ± 0.007 K. If global maps of D2 and D3 SST are differenced, the mean difference is -0.176 K. Thus, a consistent picture emerges from validation and from differencing SST fields: retrieved D3 SSTs are globally warmer than D2 SSTs by about 0.17 K. While important in its own right, this global offset between the two retrievals is not the subject of this present paper—we briefly discuss its origins in the next paragraph, and thereafter remove this relative bias empirically in order to focus on spatially variable biases.

Global biases of this magnitude are expected when using retrieval coefficients based on radiative-transfer modelling (Merchant and Le Borgne 2004). The forward-modelling process used to simulate the BTs inevitably contains systematic errors relative to reality. These may arise from errors in model parameters (such as surface emissivity, or absorptivity of radiatively active gases), from biases in the specification of the simulated states (such as assumed aerosol-loading or trace-gas concentrations) or inaccuracies in specification of the spectral response-function or calibration of the instrument. If the mean biases in the forward-modelled BTs are the elements of $\mathbf{e}$, then there is a bias in retrieved SST of $\mathbf{a}^{\mathrm{T}}\mathbf{e}$. The sum of absolute SST retrieval coefficients is always greater than one, so biases in the forward model are usually amplified by the retrieval equation (although biases with certain characteristics can be attenuated). The fact that AATSR SST biases are $\sim$0.1 K therefore implies that the forward-modelling process has been performed to an accuracy of the order of 0.01 to 0.1 K. To obtain negligible (0.01 K) biases by radiative-transfer modelling, the forward-modelling process would need to be unbiased to order 0.001 to 0.01 K; this is demonstrably not feasible with current knowledge (Merchant and Le Borgne 2004). In summary, global biases are of order 0.1 K, and manifest in absolute terms in validation and in relative terms as differences between D2 and D3 retrievals.

(*b*) *Systematic error*

We take night-time 10 arc-minute AATSR SSTs for December 2002 to May 2003, and average these over this period and in 1° latitude–longitude grid cells. The D3 SST field resulting is shown in Fig. 1, and displays the oceanic thermal features one would expect. Some ocean cells have no mean SST because they are persistently flagged during the period, because of sea-ice or detection of cloud. (In this map, the standard error in a 1°-mean SST is of order 0.02 K. For a recent discussion of systematic errors that may be present in ATSR SSTs from cloud detection, see Merchant *et al.* (2005).)

Next, the D2 $-$ D3 SST difference is formed and the global mean of this difference is removed. Thus, we form the zero-mean map of the spatially variable component of D2 $-$ D3 SST difference, shown as Fig. 2(a). Here, we have used a 5° spatial resolution, to match the resolution of the simulations with which this field will be compared. The average number of 10 arc-minute samples per grid cell over 6 months is $\sim$4000 (although considerably lower in regions of persistent cloud cover). With 10 arc-minute SSTs having a random error of about 0.3 K, this means the standard error in the mean SST for each cell is of order 0.01 K—an order of magnitude smaller than the systematic effects that we wish to explore.

The dominant spatial structure of this difference is zonal. Broadly, the difference is negative at high latitudes and over the equatorial Pacific Ocean, and is positive over the

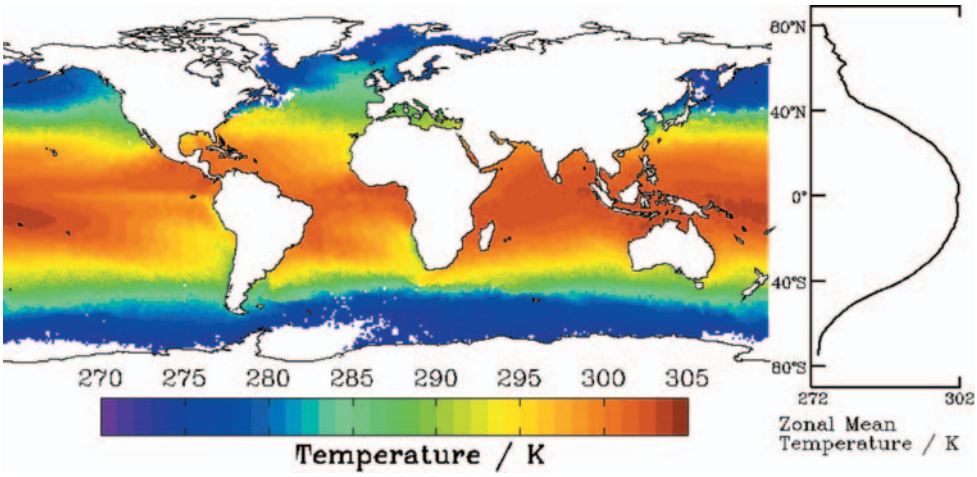

Figure 1. Mean sea surface temperature (SST) retrieved from night-time Advanced Along-Track Scanning Radiometer (AATSR) brightness temperatures for the period 1 December 2002 to 31 May 2003. The 'dual-view three-channel' (D3) retrieval algorithm was used (see text). Panel at the right-hand side shows zonal mean SST.

sub-tropics and equatorial Atlantic and Indian Ocean latitudes. The range of difference is −0.21 K to +0.20 K, with the standard deviation of 5° cell values being 0.08 K. These variations in difference are highly statistically significant compared to the random error in the mean cell values, and show a coherent spatial structure: there is therefore no doubt that they reflect systematic effects in the SST retrievals. At the right side of the map, the zonal mean difference is shown, and has a variation with latitude very similar to those noted in ATSR D2 − D3 SST differences by Merchant *et al.* (1999).

Spatially variable difference must imply, of course, spatially variable bias in at least one of the SST fields. Not having an absolute reference for SST fields that is accurate at this level, maps of bias in D2 and D3 SST cannot be directly ascertained from the observations. But we can generate such maps in simulation using a vertical profile set derived from numerical weather prediction (NWP) analyses for the same period (see appendix A for the method used). The simulated bias maps for D2 and D3 SSTs are shown in Figs. 2(b) and 2(c) respectively. Simulated zonal biases are much smaller for D3 SST than for D2 SST, as noted by Merchant (1999). The range in Fig. 2(b) is −0.25 to +0.24 K, whereas in Fig. 2(c) it is merely −0.08 to +0.04 K. The smaller systematic errors of the D3 SSTs reflect the independent information added by the 3.7 μm channel. Compared to the 11 and 12 μm channels, 3.7 μm is a cleaner window channel, being less sensitive to water vapour (although more sensitive to trace gases whose profiles are less variable).

Subtracting the D3 bias map from the D2 bias map gives us a map of simulated D2 − D3 SST difference, shown in Fig. 2(d). There is a significant degree of similarity with the observed-difference map (Fig. 2(a)). Not only are the broad zonal characteristics reproduced, but more specific meridional features are also closely matched: for example, in the Indian and Southern Oceans around 40°S. The most significant discrepancies are over the equatorial Pacific and Atlantic Oceans. The degree of similarity of Figs. 2(a) and 2(d) is represented by the correlation coefficient of 0.74 between the maps.

The most plausible explanation for the correspondence between the simulated D2 − D3 SST difference map (Fig. 2(d)) and that observed (Fig. 2(a)) is that the simulations of bias in both sorts of retrieval (Figs. 2(b) and 2(c)) are broadly realistic in

magnitude and location. This implies the presence in the SST retrievals of significant systematic errors that are not related to factors such as residual cloud contamination or excessive tropospheric aerosol; no doubt such factors do affect the SSTs, but they are not the dominant sources of systematic error overall. Nor does the presence of these systematic errors point to a mis-specification of the retrieval coefficients: these spatially variable errors arise as an intrinsic result of the linear SST retrieval method itself, rather than being a feature of any particular set of coefficients.

In the remainder of this paper, we explain the spatial structure of the SST errors presented in Fig. 2.

3. Mathematical form of systematic error

The equations of radiative transfer and the Planck function are highly nonlinear in the infra-red spectrum. Observed radiances are expressed as BTs when estimating SST because this largely linearizes the relationships between the observations and the retrieved parameter. Nonetheless, residual nonlinearity remains, and we represent this in our analysis of systematic error by formulating the forward model as an expansion up to the quadratic term:

$$\mathbf{y}^{\mathrm{o}} = \mathbf{y}_0\{\mathbf{x}_0\} + \mathbf{K}(\mathbf{x}-\mathbf{x}_0) + \begin{bmatrix} (\mathbf{x}-\mathbf{x}_0)^{\mathrm{T}}\mathbf{K}'_1(\mathbf{x}-\mathbf{x}_0) \\ \vdots \\ (\mathbf{x}-\mathbf{x}_0)^{\mathrm{T}}\mathbf{K}'_n(\mathbf{x}-\mathbf{x}_0) \end{bmatrix} + \boldsymbol{\varepsilon}^{\mathrm{o}}. \qquad (2)$$

In Eq. (2), the elements of vector $\mathbf{x}$ comprise the variables describing the geophysical state which determine the observed vector, $\mathbf{y}^o$—i.e. $\mathbf{x}$ specifies the SST and the atmospheric profiles of temperature and radiatively active gases, including water vapour. The first element of $\mathbf{x}$ is here chosen to be the SST, and will be written as x. The observation vector $\mathbf{y}^o$ lists the BTs in the three thermal channels of AATSR in each of the two view-directions. The four terms on the right-hand side of Eq. (2) are as follows:

- $\mathbf{y}_0\{\mathbf{x}_0\}$, the observation corresponding to a state $\mathbf{x}_0$, around which our forward model is expanded as a power series to second order;
- $\mathbf{K}(\mathbf{x}-\mathbf{x}_0)$, the linear component of variation of observation with state: the matrix $\mathbf{K}$ contains the first-order derivatives of the observations with respect to the state variables, and so this is the first-order term in the expansion;
- the quadratic (second-order) term, in which the matrices $\mathbf{K}'_j$ ($j = 1$ to n, where n is the dimension of the observation vector) gather the second-order partial derivatives of the expansion, including cross terms, and absorb a factor of $\frac{1}{2}$; each of the matrix multiplications $(\mathbf{x}-\mathbf{x}_0)^{\mathrm{T}}\mathbf{K}'_j(\mathbf{x}-\mathbf{x}_0)$ gives a single element; so the dimension of the column vector of these terms matches that of the observation vector;
- the measurement error vector, $\boldsymbol{\varepsilon}^o$, assumed to be a random variable, each element having zero mean and no covariance with other elements.

Hereafter, the quadratic term will not be written out fully as above, but simply as $(\mathbf{x}-\mathbf{x}_0)^{\mathrm{T}}\mathbf{K}'(\mathbf{x}-\mathbf{x}_0)$. Retaining the terms up to the quadratic term is sufficient to distinguish systematic errors that would arise in SST retrieval even if the system were linear from those that arise from nonlinearity.

With this nonlinear forward-model, we proceed with an analysis of systematic retrieval error that draws upon and extends that of Eyre (1987).

We are interested in systematic retrieval error—i.e., biases in retrieved SSTs. For any given subset of observations, the bias is the expectation (usually estimated with

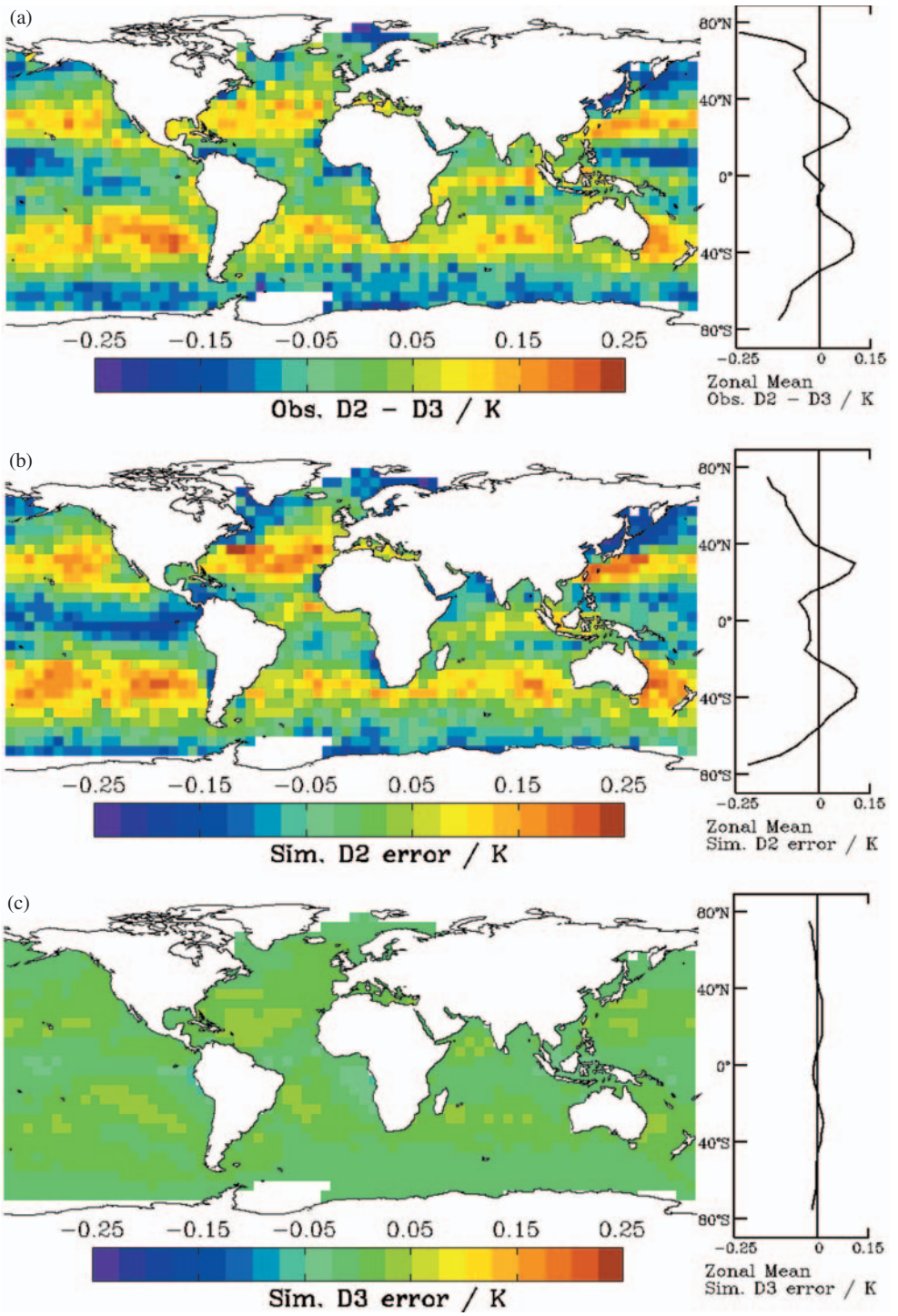

Figure 2. Systematic error in retrievals of sea surface temperature (SST): (a) difference in night-time SST retrieved using daytime 'dual-view two-channel' (D2) and night-time 'dual-view three-channel' (D3) coefficients with Advanced Along-Track Scanning Radiometer (AATSR) data; (b) simulated retrieval error in D2 retrievals of SST for a profile dataset spanning the same period as (a); (c) as (b) but for D3 retrievals, and (d) difference between simulated D2 and D3 retrievals (see text). To the right of each panel is a zonal-mean profile of the difference or simulated error (K).

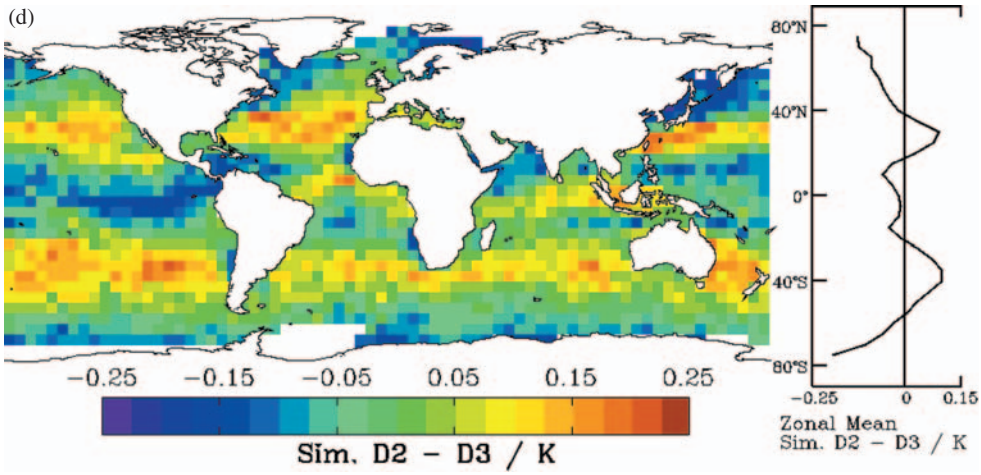

Figure 2. Continued.

the mean of a sample) of the difference between the estimated (retrieved) SST, $\widehat{x}$, and the actual SST. If the expectation of the retrieval error is taken over the full domain of observations, the answer will be zero for 'perfect' retrieval coefficients, by design. (Our AATSR SST retrievals are not 'perfect', and we have assumed that the imperfection has the form of a small global offset that we have removed in creating the D2 − D3 difference maps.) However, the global mean retrieval error can be zero while, at the same time, there are systematic errors for SSTs obtained in certain regions, seasons, etc. This is illustrated in Fig. 2(a), for example.

We use an over-bar to represent the expectation of a quantity over a subset of the domain of observations, such as a given region. We use angle brackets, $\langle\ \rangle$, to indicate a global mean—i.e. the expectation over the full domain of observations. It can be shown (see appendix B) that the form of the bias in a subset of data is:

$$\overline{\widehat{x} - x} = (\mathbf{a}^{\mathrm{T}}\mathbf{K} - \mathbf{i}^{\mathrm{T}})(\overline{\mathbf{x}} - \langle\mathbf{x}\rangle) + \mathbf{a}^{\mathrm{T}}(\overline{(\mathbf{x} - \langle\mathbf{x}\rangle)^{\mathrm{T}}\mathbf{K}'(\mathbf{x} - \langle\mathbf{x}\rangle)} - \langle(\mathbf{x} - \langle\mathbf{x}\rangle)^{\mathrm{T}}\mathbf{K}'(\mathbf{x} - \langle\mathbf{x}\rangle)\rangle). \quad (3)$$

Equation (3) describes the systematic error we expect to see in retrieved SSTs. There are two terms on the right-hand side.

The first term is linear in the difference $(\overline{\mathbf{x}} - \langle\mathbf{x}\rangle)$, and represents 'bias to the mean'. This is also referred to as 'prior error'; we use this term here. Prior error is familiar in retrieval theory from, e.g., Eyre (1987) (cf. Eq. (9) therein), particularly in the context of atmospheric soundings made using microwaves, where the equations of radiative transfer are very nearly linear and prior error is the dominant systematic error. To understand the relevance to SST retrieval, note that implicit in any regression-based set of retrieval coefficients is a state that acts as a first guess ('prior state') for the retrieval. For an unweighted regression, the prior state is the mean of the states in the regression data base. This prior state contributes to the retrieval result. If the coefficients are applied to a region and/or season that is systematically different from the prior state, the result is a systematic error because (as one can view it) the prior state is systematically in error. The prior error is linear in $(\overline{\mathbf{x}} - \langle\mathbf{x}\rangle)$ and the matrix that multiplies this difference, $(\mathbf{a}^{\mathrm{T}}\mathbf{K} - \mathbf{i}^{\mathrm{T}})$, is constant. Note that one should not infer (by analogy with a scalar equation of form constant × difference) that the more 'in error' is the prior (i.e. the greater the magnitude of $(\overline{\mathbf{x}} - \langle\mathbf{x}\rangle)$), the greater is the prior error:

the matrix multiplication leads to a sum of terms that can offset each other. We shall show, below, that, in the case of SST, the prior error changes sign and magnitude with latitude.

The second term arises because of nonlinearity, and also involves the mean departure of the subset from the prior state. This term is usually neglected in error analysis of retrievals using maximum likelihood methods (e.g., Rodgers 1990) because it is assumed that the system is sufficiently linear over the error range. This is not valid here, and we shall find that the prior error and nonlinearity error are of similar magnitudes. We shall not evaluate this nonlinear term explicitly, but will verify the approximately quadratic form of the nonlinearity error for the case of SST.

4. Analysis of SST biases

(*a*) *Prior error*

Our objectives in this section are:

- to quantify the prior error in the SST retrievals;
- to understand the geographical variation in the prior error in terms of the global variations of SST and atmospheric state; and
- to examine what portion of the total systematic error (e.g., Fig. 2(b)) is explained by the prior error.

The first two of these objectives amount to identifying and evaluating the dominant terms in the prior error, $(\mathbf{a}^{\mathrm{T}}\mathbf{K} - \mathbf{i}^{\mathrm{T}})(\overline{\mathbf{x}} - \langle\mathbf{x}\rangle)$. The most succinct way to do this is to reduce the state vector to a few parameters that determine almost all the variation in the observations, as follows. We do this for D2 SSTs only, since the retrieval errors are larger for this type of retrieval.

The BT in an atmospheric-window portion of the infrared spectrum is largely determined by the surface temperature, the total-column water-vapour present in the atmosphere, the broad vertical distribution of water vapour in the atmosphere, the tropospheric lapse-rate, and the difference between the atmospheric and surface temperature. It turns out to be the contrasting geographical variations in these features of the surface-and-atmospheric state that dominate the pattern of prior error. These features of the surface-and-atmospheric state vary on a range of scales. Broadly, total-column water-vapour over the oceans is a maximum in the equatorial zone, and reduces, with falling atmospheric temperatures, towards high latitudes. Within latitude zones, large-scale circulations (e.g., the Walker circulation) affect both the total-column and vertical distribution of water vapour, and there is considerable variability associated with the presence of land masses. Air–sea temperature difference can vary on relatively short spatial scales ($<$100 km) as the SST changes more than the temperature of the lower atmosphere around upwellings and fronts. These features are all reflected to some degree in the prior error, which can therefore be expected to have geographical variations on all these scales.

To quantify the prior error as simply as possible, we represent the state by a state vector comprising the SST, the amplitudes of the leading three empirical orthogonal functions (EOF)s of the profile of surface–atmosphere temperature difference, and the amplitudes of the four leading EOFs of the water-vapour mixing-ratio profile. These are estimated from the same set of profiles as were used in the simulations for Figs. 2(b,c and d). A linear forward-model, $\mathbf{K}$, for the observations in terms of this reduced state-vector is also needed. The linear model that explains the maximum fraction of the total variance in the observations is found by multiple linear regression of the (simulated) observations to the elements of the reduced state-vector. The element (i, j) of $\mathbf{K}$ is the

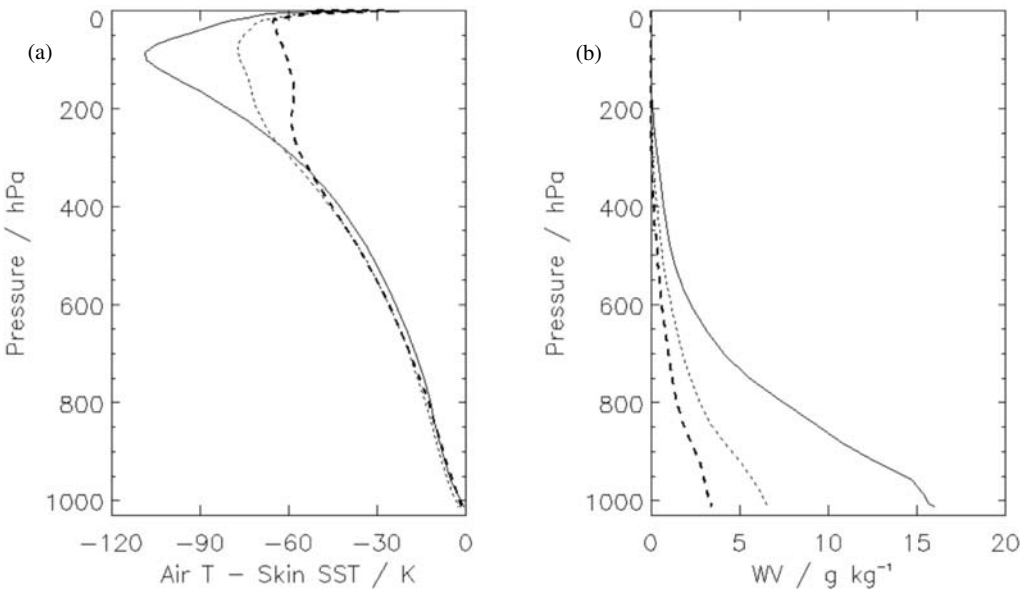

Figure 3. Evaluating biases in sea surface temperature—zonal-mean vertical profiles used for the evaluation of 'prior error' (see text): (a) atmospheric minus surface temperature (K), and (b) water-vapour mass mixing-ratio (g kg^{-1}). Solid lines denote 'tropical', light dashed lines 'mid-latitude' and heavy dashed lines 'high latitude'.

gradient found in the multiple linear regression expressing the rate of change of the ith observation with respect to the jth parameter in the state vector. More detail about the EOFs and the linear forward-model is given in appendix C.

To illustrate the evaluation of prior error for some concrete cases, we consider D2 SST retrieval applied to three profiles that are zonal averages over latitude ranges 10°N to 15°N, 35°N to 40°N and 60°N to 65°N (i.e. tropical, mid-latitude and high latitude examples). The profiles are shown in Fig. 3. For each of these profiles, we calculate the corresponding reduced state-vector, and then evaluate the first term on the right-hand side of Eq. (3). The components of this evaluation are shown in Table 1. The table gives us insight into how the D2 retrieval coefficients act to minimize the global error in retrieved SST. There is a contribution to prior error from the difference of each element of the state vector from its mean value. For each profile, we can see that these contributions to prior error tend to cancel each other to some degree, with the contribution from $x - \langle x \rangle$ being of one sign and the other contributions mostly being of opposite sign. However, the elements of the state vector have different and complex geographical variations and the prior error is a fixed linear combination of the elements of $(\overline{\mathbf{x}} - \langle \mathbf{x} \rangle)$, and thus the cancellation is not, in general, exact: the prior error is in general non-zero. This is illustrated further in Fig. 4, which shows the latitudinal variation of the contributions to prior error from the most significant elements of the state vector. Each curve is proportional to the difference of a geophysical variable from its global mean. (The variables drawn are the SST, the first EOF of the temperature profile, and the first and second EOFs of the water-vapour profile.) We can see how the contribution to prior error of the SST tends to be cancelled at a given latitude by the sum of the other contributions, but imperfectly, leading to the relatively complex latitudinal distribution of the total prior error (also shown).

TABLE 1. EVALUATION OF D2 PRIOR ERROR FOR PROFILES SHOWN IN FIG. 3

		$\langle \mathbf{x} \rangle$	$\overline{\mathbf{x}}$	$(\overline{\mathbf{x}} - \langle \mathbf{x} \rangle)$	$(\mathbf{a}_{D2}^{T}\mathbf{K} - \mathbf{i})$	Product
Tropical (10°N–15°N)	x/K	291.4	300.3	8.87	0.0188	0.167
	e_{T1}	0.0	−0.630	−0.630	0.0698	−0.044
	e_{T2}	0.0	0.705	0.705	−0.0452	−0.032
	e_{T3}	0.0	−0.195	−0.195	−0.0019	0.000
	e_{W1}	0.0	−0.772	−0.772	0.0920	−0.071
	e_{W2}	0.0	0.901	0.901	−0.0999	−0.090
	e_{W3}	0.0	0.092	0.092	−0.0018	0.000
	e_{W4}	0.0	0.192	0.192	−0.0469	−0.009
				Prior error		−0.079
				(Sum of column above)		
Mid-latitude (35°N–40°N)	x/K	291.4	288.1	−3.34	0.0188	−0.063
	e_{T1}	0.0	−0.092	−0.092	0.0698	−0.006
	e_{T2}	0.0	−0.663	−0.663	−0.0452	0.030
	e_{T3}	0.0	0.026	0.026	−0.0019	0.000
	e_{W1}	0.0	0.661	0.661	0.0920	0.061
	e_{W2}	0.0	−0.326	−0.326	−0.0999	0.033
	e_{W3}	0.0	0.169	0.169	−0.0018	0.000
	e_{W4}	0.0	0.038	0.038	−0.0469	0.002
				Prior error		0.052
				(Sum of column above)		
High latitude (60°N–65°N)	x/K	291.4	277.4	−14.06	0.0188	−0.265
	e_{T1}	0.0	0.687	0.687	0.0698	0.048
	e_{T2}	0.0	−0.888	−0.888	−0.0452	0.040
	e_{T3}	0.0	−0.304	−0.304	−0.0019	0.001
	e_{W1}	0.0	1.111	1.111	0.0920	0.102
	e_{W2}	0.0	−0.625	−0.625	−0.0999	0.062
	e_{W3}	0.0	0.381	0.381	−0.0018	−0.001
	e_{W4}	0.0	−0.255	−0.255	−0.0469	0.011
				Prior error		0.000
				(Sum of column above)		

For definitions of variables, see main text. The values in the column headed 'Product' are the products of the two columns immediately to the left, and are the components of the inner product $(\mathbf{a}^{T}\mathbf{K} - \mathbf{i}^{T})(\overline{\mathbf{x}} - \langle \mathbf{x} \rangle)$, which is the expression for prior error.

The range of the zonal prior error is from −0.08 to +0.05 K, rather less than the zonal retrieval error in D2 retrievals simulated in Fig. 2(b), which ranges from −0.19 to +0.09 K. The zonal prior error curve accounts for 15% of the variance in the curve of zonal retrieval error. This suggests that the prior error term is significant, but not dominant. The remainder of the retrieval error is due to the effects of nonlinearity.

(*b*) *Bias from nonlinearity*

We may attribute differences between the prior error and systematic error to nonlinearity in the equations of radiative transfer. (This is represented, to second order, by the second term in Eq. (B.6).) In principle, one could estimate the $\mathbf{K}'_j$ matrices and create a quadratic forward-model, as expressed by Eq. (2). Here, we use the difference between simulated systematic error and estimated prior error to make an estimate of the nonlinearity error, and verify that the form of the nonlinearity error is predominantly quadratic. Again, we present the case of D2 SST retrieval.

For each NWP profile we subtract the prior error (estimated as in subsection 4(a)) from the simulated retrieval error in D2 SST (as calculated for Fig. 2(b)), giving an estimate of the nonlinearity error. The zonal-mean nonlinearity-error thus found is shown in Fig. 5 (along with the systematic error and prior error).

If Eq. (2) is sufficient to describe the degree of nonlinearity, then the nonlinearity error should have the form of the second term on the right side of Eq. (B.6).

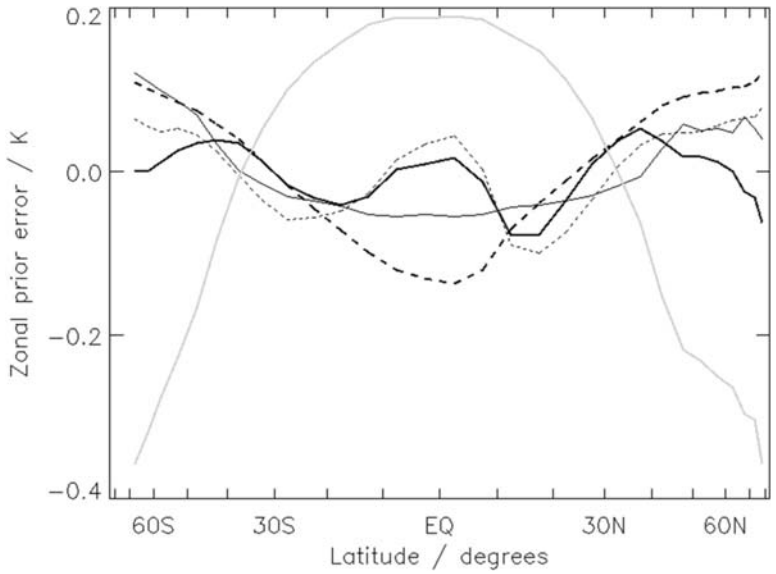

Figure 4. Dependence on latitude of contributions to zonal-mean prior error (K) in retrievals using the daytime 'dual-view two-channel' (D2) coefficients (see text), calculated on latitude bands 5° in width and plotted on an area-proportional scale: contribution from deviations from global mean sea surface temperature (light grey solid line); contribution from first empirical orthogonal function (EOF) of atmospheric temperature profile (thin solid line); contribution from first EOF of atmospheric water-vapour profile (thick dashed line); contribution from second EOF of atmospheric water-vapour profile (thin dashed line) and total prior error (i.e. the sum of the contributions mentioned above, plus minor contributions not shown in this diagram) (solid black line).

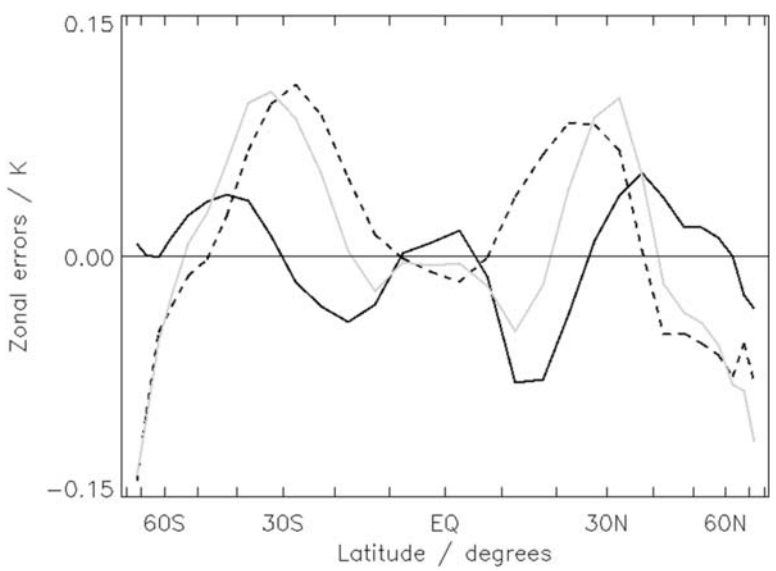

Figure 5. Dependence on latitude of elements of zonal-mean error (K) in retrievals using the daytime 'dual-view two-channel' (D2) coefficients (see text): systematic error (grey line); prior error (black line) and nonlinearity error (difference of systematic and prior errors) (dashed line).

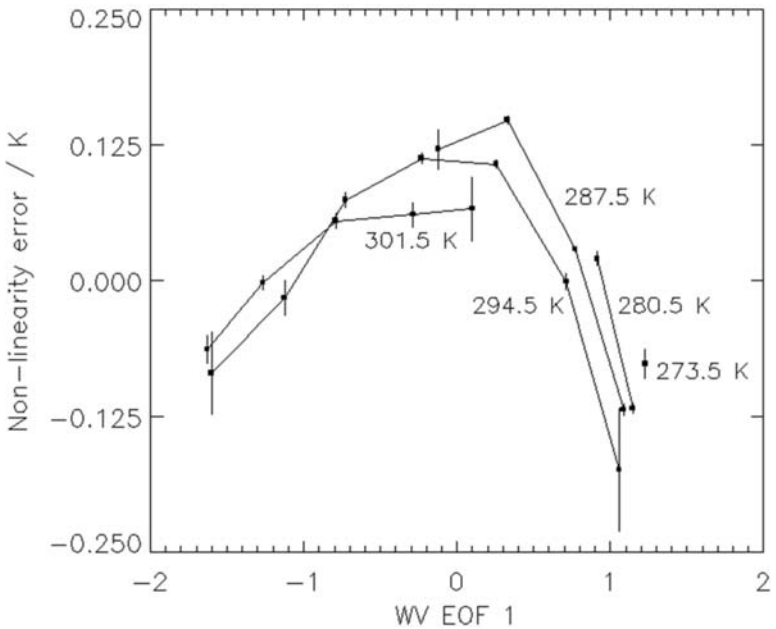

Figure 6. Average nonlinearity error as a function of the amplitude of the first empirical orthogonal function (EOF) of the water-vapour profile (e_{W1}) for different ranges of sea surface temperature (SST). Each curve covers a range of SST 7 K wide and is labelled with the value of the centre of the range. Not all values of e_{W1} occur for all SST ranges: very wet atmospheres (negative e_{W1}) are associated only with relatively high SSTs. Vertical bars show the standard error in the average nonlinearity error for given ranges of SST and e_{W1}.

Looking at this term, it is apparent that if only one element in **x** is varied, the corresponding variation in nonlinearity error should be quadratic (i.e. is a parabola). To explore this, we stratify the set of profiles with respect to two state-vector variables, SST and the amplitude of the first water-vapour EOF (e_{W1}), and discard all profiles with any other state-vector variable (i.e. any other EOF amplitude) outside the range -0.5 to $+0.5$. The retained profiles' nonlinearity errors are then averaged within each stratum of SST and e_{W1}. This has the effect of (approximately) retaining variations in only two elements of the state vector. The results are given in Fig. 6, and each curve is clearly not linear. The SST stratum with the most complete range of e_{W1} is that covering 291 to 298 K (centre value = 294.5 K), and we test the form of the nonlinearity on this curve by fitting to it a quartic polynomial. The linear and quartic coefficients are not statistically different from zero at the 2σ level; for the linear coefficient this is expected, since the linear error is the prior error which we have already removed. Over the available range of e_{W1}, the curve is dominated by the quadratic term (which accounts for 80% of the curve's variance), although the cubic term is statistically significant. From this we can infer that Eqs. (2) and (3) are fair approximations to the forward-model and error-structure of SST retrievals, although third-order terms also contribute significantly.

Lastly, we note that, in a qualitative sense, Fig. 6 explains the latitudinal variation of the nonlinearity error shown in Fig. 5. In general, moving polewards of the equator in Fig. 5 corresponds to moving from states more typical of the left-side of Fig. 6 to states more typical of the right-side of Fig. 6, hence the double-peaked nature of the curve of zonal nonlinearity error in Fig. 5.

5. Discussion

Retrieval of SST using linear coefficients is simple and effective. We have shown that, nonetheless, the systematic errors introduced in the process of retrieval are complex, and not always negligible. One term in the bias, the prior error (or the bias to the prior state), is linearly related to modes of variability in SST and in the atmosphere. In addition, there is a second bias-term that seems to be well represented by a quadratic form, and arises because the relationships are not linear between BTs, SST and atmospheric state. For both terms, the spatial patterns of bias reflect geographical variation in the mean state. As a result, the biases show texture at scales of 5° of latitude and of longitude.

In this case study, we have analysed the bias for an atypical SST sensor (in that it is a dual-view instrument) to whose observations are applied a global set of constant coefficients for SST estimation. Single-view sensors are more typical, and the use of weakly nonlinear retrieval coefficients (e.g., Brisson *et al.* 2002) is common when retrievals are made using the split-window channels (11 μm and 12 μm). Coefficients are sometimes regionally defined (e.g., for certain latitude zones) or otherwise stratified (e.g., by estimated total-column water-vapour: Barton (1998)). These departures from using global linear coefficients are all attempts to reduce bias in the retrieved SST. The nonlinear split-window SST has been widely adopted, whereas other approaches are less widespread. None of these schemes, to our knowledge, has been subjected to a systematic characterization of the retrieval biases such as we have attempted here. Understanding the retrieval biases is the logical basis for progress in reducing or correcting for them. We intend to turn to the bias characteristics of other sensors in future papers.

The understanding of the SST biases developed here could be obtained only by use of forward modelling (although the equations apply equally well to empirical coefficients). By comparing relative biases between retrievals in simulation and reality, we were able to demonstrate that our forward-modelling capability was adequate to simulate subtle bias characteristics. This strengthens the case for use of radiative-transfer modelling for developing SST retrieval schemes.

We have characterized the biases for AATSR dual-view retrievals, but we have not addressed how those biases should be reduced or corrected in developing a climate-quality SST time-series. It is our intention to turn to that question also in a future article.

Acknowledgements

AATSR data are copyright European Space Agency (ESA) and were provided within the framework of the ENVISAT cal/val activities.

Appendix A

Simulation of SST biases

Simulated maps of retrieval bias and differences between D2 and D3 SSTs are derived using procedures intended to make them comparable to the observed fields, as follows. We obtain Met Office NWP analysis fields at approximately 1° resolution over the global ocean for the 1st, 11th and 21st of each month (or dates closest to these if there are data availability problems) between December 2002 and May 2003 inclusive (thus matching the observed period). NWP profiles with relative humidity exceeding 95% in any tropospheric layer are deemed cloudy, and excluded. This was a rule used by

Merchant *et al.* (1999) as a means of sampling NWP profiles so that the retained profiles represent the clear-sky conditions for which SST retrievals can be made. We retain this pragmatic approach, since it has served reasonably well for defining SST coefficients, and we have no better-founded alternative. This gives us about 24 000 profiles sampled in a way that broadly reflects the sampling in the observed SST maps.

Since this is a large number of profiles, simulation using a line-by-line radiative-transfer model is unfeasible. Instead, we use the fast forward-model, RTTOV-7 (Saunders *et al.* 2002) to generate AATSR BT simulations. Comparisons of RTTOV-7 with spectrally resolved models have shown that for typical SST sensor channels, the resulting brightness-temperatures differ typically by ∼0.1 K in the mean and with a scatter of ∼0.1 K (Merchant and Le Borgne 2004). This degree of mismatch between RTTOV-7 and the spectrally resolved model used for deriving coefficients would itself introduce systematic errors that are comparable to those we are trying to investigate, were we to apply the standard coefficients to the RTTOV-7 BTs. However, the mismatch is small enough for us to expect error characteristics in the simulation to be similar to those in reality, if we use coefficients that have a comparable derivation to the standard coefficients and are consistent with the simulated BTs to which they are to be applied—i.e. the coefficients need to be obtained from the same fast model. Therefore, we also run RTTOV-7 on the profile set used for defining SST coefficients, and obtain, using the standard procedures, new coefficients that are only intended for use with BTs from RTTOV-7. These retrieval coefficients are applied to the global simulated BTs, and, by taking the difference with the profile SST, the simulated SST retrieval error is found for each of the ∼24 000 profiles. In this case, the global mean simulated retrieval-error is negligibly different from zero (as it should be), so there is no correction of a global offset. Aggregation into 5° cells then gives us maps of simulated SST bias. This is all done for both the centre and edge of the swath, and the final step is to form the appropriate weighted average of the centre and edge results.

APPENDIX B

Derivation of systematic error

The basic linear regression equations for deriving the SST coefficients may be written, using the symbols of Merchant *et al.*, (1999), as

$$\begin{aligned} \mathbf{a}^{\mathrm{T}} &= \mathbf{S}_{\mathbf{yy}}^{-1}\mathbf{s}_{x\mathbf{y}} \\ a_0 &= \langle x \rangle - \mathbf{a}^{\mathrm{T}}\langle \mathbf{y}^o \rangle \end{aligned} \tag{B.1}$$

where $\mathbf{S}_{\mathbf{yy}}$ is the covariance matrix of observation vectors, $\mathbf{s}_{x\mathbf{y}}$ is the vector of covariances of SSTs and observation vectors, and angle brackets indicate a global average over 'observations' (whether simulated or measured). We choose the linearization point for the forward model to be the mean state in this averaging:

$$\langle \mathbf{x} \rangle = \mathbf{x}_0. \tag{B.2}$$

This choice is not necessary, but it conveniently removes an offset term from subsequent steps. From Eqs. (2) and (B.2) we have

$$\langle \mathbf{y}^o \rangle = \mathbf{y}_0\{\mathbf{x}_0\} + \langle (\mathbf{x} - \mathbf{x}_0)^{\mathrm{T}}\mathbf{K}'(\mathbf{x} - \mathbf{x}_0) \rangle, \tag{B.3}$$

where the second term on the right would not exist in the linear case.

Substituting a_0 deduced from Eq. (B.1) into Eq. (1), and then using Eq. (B.3), we find the retrieval is equivalent to

$$\widehat{x} = \langle x \rangle + \mathbf{a}^{\mathrm{T}}(\mathbf{y}^o - \langle \mathbf{y}^o \rangle) = \langle x \rangle + \mathbf{a}^{\mathrm{T}}(\mathbf{y}^o - \mathbf{y}_0 - \langle (\mathbf{x} - \mathbf{x}_0)^{\mathrm{T}} \mathbf{K}' (\mathbf{x} - \mathbf{x}_0) \rangle). \tag{B.4}$$

Substituting for $\mathbf{y}^o$ from Eq. (2) and subtracting the true SST, x, gives

$$\begin{aligned} \widehat{x} - x = {} & (\mathbf{a}^{\mathrm{T}}\mathbf{K} - \mathbf{i}^{\mathrm{T}})(\mathbf{x} - \mathbf{x}_0) + \mathbf{a}^{\mathrm{T}}\boldsymbol{\varepsilon}^o \\ & + \mathbf{a}^{\mathrm{T}}((\mathbf{x} - \mathbf{x}_0)^{\mathrm{T}} \mathbf{K}' (\mathbf{x} - \mathbf{x}_0) - \langle (\mathbf{x} - \mathbf{x}_0)^{\mathrm{T}} \mathbf{K}' (\mathbf{x} - \mathbf{x}_0) \rangle), \end{aligned} \tag{B.5}$$

where $\mathbf{i}^{\mathrm{T}} = [1, 0, \ldots 0]$. This describes the error in SST for a particular retrieval where the true state is $\mathbf{x}$. Our final step is to consider the mean error for some subset of cases, such as for a latitude zone, region, and/or a particular season. If we represent averaging over that subset with an overbar (and assume the averaging is sufficient to render random error negligible) we obtain our expression for systematic error

$$\overline{\widehat{x} - x} = (\mathbf{a}^{\mathrm{T}}\mathbf{K} - \mathbf{i}^{\mathrm{T}})(\overline{\mathbf{x}} - \mathbf{x}_0) + \mathbf{a}^{\mathrm{T}}(\overline{(\mathbf{x} - \mathbf{x}_0)^{\mathrm{T}} \mathbf{K}' (\mathbf{x} - \mathbf{x}_0)} - \langle (\mathbf{x} - \mathbf{x}_0)^{\mathrm{T}} \mathbf{K}' (\mathbf{x} - \mathbf{x}_0) \rangle). \tag{B.6}$$

In the main text, Eq. (B.6) is re-expressed using Eq. (B.2).

APPENDIX C

Reduced-state vector and linear forward-model

To define the reduced state-vector and linear forward-model, we use the set of NWP profiles and simulated observations as described in appendix A. The mean profiles of atmospheric–surface temperature difference (T_{air}) and of water-vapour mass-mixing-ratio (W) are shown in Fig. C.1. The mean SST in the set is 291.4 K.

The sensitivity of the observed BTs to water vapour and atmospheric temperature is a function of altitude, as shown in Fig. C.2. To obtain an efficient reduced state-vector (with few elements), we weight the variability at each level in the NWP profiles according to the sensitivity of BT to that variability (subject to a minimum weight to avoid division-by-zero). The averages (over channels and view angles) of $\mathrm{d}y/\mathrm{d}T_{\mathrm{air}}$ and $\mathrm{d}y/\mathrm{d}W$ were used for this weighting when calculating the EOFs of the temperature difference and water-vapour profiles respectively.

For the profile of temperature difference, the first three EOFs are found to account for 52.7%, 33.1% and 6.2% of the weighted variance respectively. These EOFs are shown in Fig. C.3. The four leading EOFs of the water-vapour profiles account for 85.6%, 8.6%, 2.4% and 1.2% of the weighted variance, and are also shown in Fig. C.3.

The linear model is found by multiple linear regression of the BT of each channel in each view against the skin SST and the amplitudes of the leading EOFs of the temperature and water vapour profiles. The elements of $\mathbf{K}$ are the gradient coefficients thus obtained, and represent estimates of the global-mean total derivative of the observations (BTs) with respect to state variables (such as SST). This contrasts with $\mathbf{K}$ matrices defined physically for use in retrieval in linear systems and for use for local error analysis in nearly-linear systems (e.g., Rodgers 1990), where the elements of $\mathbf{K}$ are evaluations of the partial derivatives of the observations with respect to state variables. Here, we require a linear model applicable over the global range of a mildly nonlinear system, since we are investigating the error characteristics of globally applied linear retrieval coefficients. To avoid over-fitting, only as many EOFs were retained in the state vector

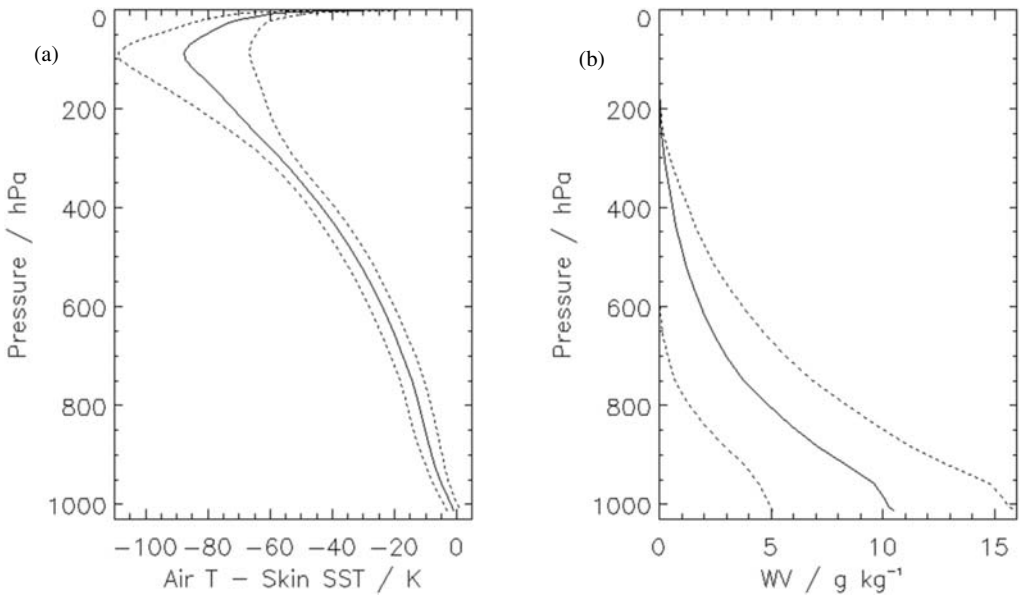

Figure C1. Vertical profiles of global means (solid lines) and global variability (dashed lines denote plus and minus one standard deviation) in Met Office numerical weather predictions of the state of the global atmosphere (see appendix A): (a) atmospheric temperature minus sea surface temperature (K), and (b) water-vapour mass mixing-ratio (g kg^{-1}).

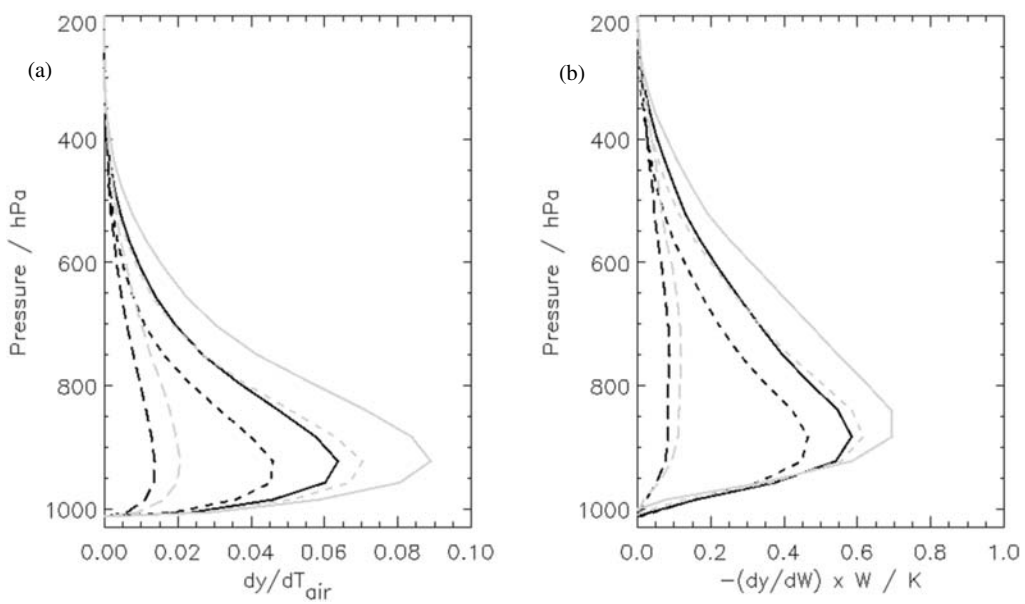

Figure C2. Sensitivity of top-of-atmosphere brightness-temperature (y) in different views to changes in: (a) atmospheric temperature and (b) water-vapour volume mixing-ratio (W). For visual clarity, the rate of change of y with respect to the fractional change in W has been shown rather than $\mathrm{d}y/\mathrm{d}W$ itself. Solid lines denote the 12 μm channel; short-dashed lines the 11 μm channel; long-dashed lines the 3.7 μm channel; heavy lines the nadir view, and light lines the forward view at 55.6°. Calculations were performed on pressure levels used in the Radiative Transfer for TIROS Operational Vertical Sounder (RTTOV-7) fast forward model developed by Saunders *et al.*

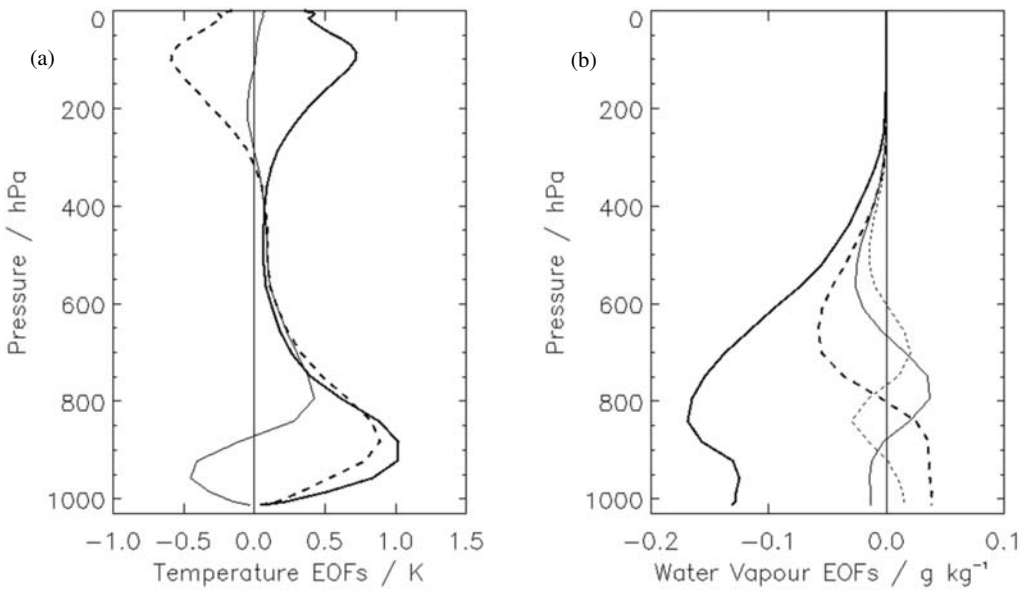

Figure C3. Leading empirical orthogonal functions (EOFs) of variability in weighted atmospheric profiles: (a) EOFs of profiles of surface-minus-atmospheric temperature, and (b) EOFs of water-vapour profiles. Heavy solid lines denote the first EOF, heavy dashed lines the second, light solid lines the third and light dashed lines the fourth EOF ((b) only). The weighting accounts for the sensitivity of brightness temperatures shown in Fig. C.2. We adopt the convention that the amplitudes of the EOFs are non-dimensional, and have unit variance, and that the EOFs have dimension. The temperature EOFs (K) emphasize the structure in the lower troposphere, where the sensitivity (Fig. C.2) is greatest. They also have features around the tropopause, where the global variability in atmosphere-surface temperature difference is greatest. These features arise because of co-variations of lower-tropospheric lapse-rate and tropopause height, and are of little significance to the forward model. The water-vapour (W) EOFs (g kg^{-1}) emphasize variability around 800 hPa, where both the sensitivity of observations to W and the variability of W are high.

as have slope coefficients that are statistically significant at the 3σ level for all channels and views. As a result, the state vector consists of the skin SST, the amplitudes of the three leading EOFs of the profile of surface-atmosphere temperature difference, and the amplitudes of the four leading EOFs of the water-vapour mixing-ratio profile. This linear forward-model fits the observations with the standard deviation of residual BTs ranging from 0.08 K in the 3.7 μm channel nadir view to 0.58 K in the 12 μm channel forward view. The residuals have both a pseudo-random component (scatter) and systematic component (unfitted nonlinearity).

The elements of **K** are shown in Table C.1 below. The elements are interpretable in terms of aspects of radiative transfer for the different channels. For example

• Gradients with respect to SST are close to unity, reflecting the fact that, globally, observed BTs closely follow the SST. (In contrast, the partial derivative of BT with respect to SST can be much lower than unity where atmospheric absorption is great.)

• The gradients with respect to the first EOF of the temperature difference profile (row e_{T1}) are positive because this EOF represents a warming of the atmospheric column, reducing the differential between the radiance absorbed and emitted by the atmosphere, and thus increasing the BT.

• The gradients with respect to the first EOF of the water-vapour profile, e_{W1}, are positive because a positive coefficient of this EOF reduces the tropospheric water-vapour loading, thereby reducing the absorption of upwelling radiance in the atmosphere and

TABLE C1. ELEMENTS OF MATRIX **K**

Slope with respect to:	12 μm 0°	11 μm 0°	3.7 μm 0°	12 μm 55.6°	11 μm 55.6°	3.7 μm 55.6°
x	0.985	1.002	0.981	0.977	0.993	0.967
e_{T1}	0.419	0.320	0.104	0.613	0.469	0.155
e_{T2}	0.477	0.314	0.160	0.713	0.495	0.254
e_{T3}	0.042	0.009	0.024	0.104	0.036	0.045
e_{W1}	2.918	2.209	0.632	3.595	2.943	0.844
e_{W2}	0.502	0.299	0.146	0.772	0.496	0.218
e_{W3}	0.234	0.157	0.062	0.316	0.221	0.083
e_{W4}	0.182	0.119	0.038	0.242	0.178	0.053

The elements are estimates of the global rates of change of BTs in AATSR window channels at the satellite zenith angles indicated, with respect to the parameters in the reduced state-vector. x is SST; e indicates the expansion coefficient for a particular EOF; in the subscripts of e, T indicates an EOF of the temperature difference profile, W indicates an EOF of the water-vapour profile, and the number is the index of the EOF.

increasing the BT. The magnitude of the gradient with respect to e_{W1} is less for the 3.7 μm channel than for the 11 μm and 12 μm channels partly because water-vapour absorption is less in the former window; and is greater for the forward view (55.6°) than at nadir because the forward view has a longer path through the atmosphere, and thus absorption by water vapour is greater.

REFERENCES

Barton, I. J. 1998 Improved techniques for the derivation of sea surface temperatures from ATSR data. *J. Geophys. Res.*, **103,** 8139–8152

Brisson, A., Le Borgne, P. and Marsouin, A. 2002 Results of one year of preoperational production of sea surface temperatures from GOES-8. *J. Atmos. Oceanic Technol.*, **19,** 1638–1652

Eyre, J. R. 1987 On systematic errors in satellite sounding products and their climatological mean values. *Q. J. R. Meteorol. Soc.*, **113,** 279–292

Llewellyn-Jones, D. T., Minnett, P. J., Saunders, R. W. and Závody, A. M. 1984 Satellite multichannel infrared measurements of sea surface temperature of the N.E. Atlantic Ocean using AVHRR/2. *Q. J. R. Meteorol. Soc.*, **110,** 613–631

McClain, E. P., Pichel, W. G. and Walton, C. C. 1985 Comparative performance of AVHRR-based multichannel sea surface temperatures. *J. Geophys. Res.*, **90,** 11587–11601

McMillin, L. M. 1975 Estimation of sea surface temperatures from two infrared window measurements with different absorption. *J. Geophys. Res.*, **80,** 5113–5117

Merchant, C. J. 1999 'Eliminating bias in satellite retrievals of sea surface temperature'. PhD Thesis, University College, London, UK

Merchant, C. J. and Le Borgne, P. 2004 Retrieval of sea surface temperature from space based on modeling of infrared radiative transfer: Capabilities and limitations. *J. Atmos. Oceanic Technol.*, **22,** 1734–1746. doi: 10.1175/JTECH1667.1

Merchant, C. J., Harris, A. R., Murray, M. J. and Závody, A. M. 1999 Toward the elimination of bias in satellite retrievals of skin sea surface temperature 1. Theory, modeling and inter-algorithm comparison. *J. Geophys. Res.*, **104,** 23565–23578

Merchant, C. J., Harris, A. R., Maturi, E. and MacCallum, S. 2005 Probabilistic physically-based cloud screening of satellite infrared imagery for operational sea surface temperature retrieval. *Q. J. R. Meteorol. Soc.*, **131,** 2735–2755

Rodgers, C. D. 1990 Characterization and error analysis of profiles retrieved from remote sounding measurements. *J. Geophys. Res.*, **95,** 5587–5595

Saunders, R. W., Brunel, P., Chevallier, F., DeBlonde, G., English, S. J., Matricardi, M. and Rayer, P. J. 2002 'RTTOV-7 – Science and Validation Report'. NWP Technical Report No. 387, Met Office, UK. (Available from the National Meteorological Library, FitzRoy Road, Exeter, UK.)

Walton, C. C., Pichel, W. G., Sapper, J. F. and May, D. A. 1998 The development and operational application of nonlinear algorithms for the measurement of sea surface temperatures with the NOAA polar-orbiting environmental satellites. *J. Geophys. Res*., **103,** 27999–28012

Závody, A. M., Mutlow, C. T. and Llewellyn-Jones, D. T. 1995 A radiative-transfer model for sea surface temperature retrieval for the along-track scanning radiometer. *J. Geophys. Res*., **100,** 937–952